Front. Phys. 10(6), 107104 (2015)
DOI 10.1007/s11467-015-0509-6

RESEARCH ARTICLE

First-principles study of structural, elastic, and electronic properties of CeB_6 under pressure

Mei Tang[1], Lei Liu[1], Yan Cheng[1,2,†], Guang-Fu Ji[3]

[1] *Institute of Atomic and Molecular Physics, College of Physical Science and Technology, Sichuan University, Chengdu 610065, China*

[2] *Key Laboratory of High Energy Density Physics and Technology of Ministry of Education, Sichuan University, Chengdu 610064, China*

[3] *National Key Laboratory for Shock Wave and Detonation Physics Research, Institute of Fluid Physics, Chinese Academy of Engineering Physics, Mianyang 621900, China*

Corresponding author. Email: †ycheng@scu.edu.cn

Received July 5 2015; accepted September 10, 2015

We performed a first-principles study of the electronic, elastic, and thermal properties of the rare-earth hexaboride CeB_6 using the local density approximation (LDA) in consideration of the effective onsite Coulomb parameter U_{eff}. To systemically evaluate the effect of U_{eff} on the structure of the material, the dependences of the lattice parameter a_0 and bulk modulus B on U_{eff} were examined in the framework of the LDA+U and GGA(PBE)+U scheme. We obtained a lattice constant a_0, elastic constants C_{ij}, and a bulk modulus B at 0 K and 0 GPa that were in good agreement with the experimental results and other theoretical findings. We focused on the electronic structure by analyzing the variation of the density of states with different U_{eff} values and pressures, which indicates the metallic characteristic of CeB_6. Interestingly, the effect of high pressure was similar to that of increasing U_{eff}, as the peaks at the bottom of the conduction band moved to the high-energy region in both cases. The elastic constants C_{ij}, bulk modulus B, shear modulus G, Young's modulus E, shear-sound velocity V_S, and longitudinal-sound velocity V_L were calculated from 0 to 120 GPa. Additionally, the Debye temperature Θ_D and elastic Debye temperature Θ_E were systematically calculated using the thermodynamic methods in the range of 0–100 GPa. This research may provide a comprehensive understanding of the Kondo compound CeB_6 and similar rare-earth hexaborides.

Keywords CeB_6, structural properties, elastic properties, thermal properties, electronic structure

PACS numbers 71.15.mb, 71.20.-b

1 Introduction

Cerium compounds, in which additional electron is a strongly correlated f electron on the Ce center upon the reduction of Ce(IV) to Ce(III) [1], attract considerable research interest. The pressure dependences of the structural and elastic properties of Ce_2O_3 [2] and the electronic and magnetic structures of $Ce_2O_2FeSe_2$ [3] have been investigated recently. CeB_6 has also been intensively studied because of its interesting low-temperature magnetic phases. Experimentally, CeB_6 exhibits an antiferromagnetic order below $T_N = 2.3$ K [4], in advance of another phase transition at $T_Q = 3.2$ K, in which the order parameter remains unknown from standard experimental probes such as neutron diffraction [5, 6]. No structural phase transition occurs when the applied pressure is up to 85 GPa, but there is a possibility of structural changes in the pressure range of 85–122 GPa [7]. Remarkably, significantly different values were reported for the elastic constants; for example, the reported experimental values for C_{12} include 16, 19, 53, and 93 GPa [8–10].

The structural properties of CeB_6 were theoretically investigated using the plane-wave pseudopotential approach [11]. Sikora *et al.* [12] performed a symmetry analysis of the antiferroquadrupolar order in this substance. Recently, special attention has been directed to the magnetic moment from the $4f$ electron [13, 14], thermodynamic properties [15], and electronic structure [16]. To further understand CeB_6, the effective onsite Coulomb parameter U_{eff} must be introduced, which yields a drastic improvement in the description of the reduced ceria

[17, 18]. Because U_{eff} strongly influences the calculated observables, its optimal value remains under debate. Recently, researchers investigated the Kondo effect in CeB_6, including the observation of a Ce-resonance and its origin [19, 20].

The main objective of this work was to study the electronic structure of CeB_6 by analyzing the density of states (DOS) and elastic constants from 0 to 120 GPa under different U_{eff} and pressure values in order to understand the effects of the pressure. Furthermore, we investigated the electronic structure and thermal properties of CeB_6 from the viewpoint of the U_{eff} effect. The remaining parts of the paper are arranged as follows. In Section 2, we provide the computational details. Section 3 presents our results and discussion, and we conclude the paper in Section 4.

2 Computational details

The calculations were performed using the Cambridge Sequential Total Energy Package [21, 22]. The local density approximation (LDA) proposed by Vosko *et al.* [23] for the exchange-correlation potential was used in the LDA+U variant, where the orbital-dependent LDA+U functional form is given as

$$E_{LDA+U} = E_{LDA} + \frac{U-J}{2}\sum_{\sigma}[\mathrm{tr}\rho^{\sigma} - \mathrm{tr}(\rho^{\sigma}\rho^{\sigma})]. \quad (1)$$

Here, ρ^{σ} is the density matrix of the f states, and U and J are the Coulomb energy and the exchange energy, respectively. As described in this paper, the two energy parameters integrate into a single meaningful parameter U_{eff} ($U_{eff} = UJ$). This method can be regarded as the introduction of a penalty function that disapproves of non-integer occupation numbers of the onsite density matrix. More information about this functional is found in Refs. [24, 25].

Plane-wave basis sets were used with an energetic cutoff of 420 eV. For integration within the Brillouin zone, a 9 × 9 × 9 Monckhorst-Pack grid [26] was used. We employed the on-the-fly pseudopotential for the interactions of the electrons with the ion cores and regarded the atomic levels of $4f^1 5s^2 5p^6 5d^1 6s^2$ and $2s^2 2p^1$ as the valence electron states for the Ce and B atoms, respectively. In the structure optimization, the criteria for convergence were set as 1×10^{-5} eV/atom for the energy, 0.03 eV/Å for the force, 0.05 GPa for the stress, and 0.001 Å for the ionic displacement. To efficiently obtain self-consistency, the density-mixing scheme reported by Kresse and Furthmüller [27] is recommended for metallic systems. The spin-orbit interaction apparently has little influence on the structural properties, leading to the speculation that it is strongly atomic in nature and that transformations with geometry are non-essential with the accuracy of current DFT methods, as indicated by Pickard *et al.* [11]. Thus, we neglected the spin-orbit coupling in our study. All of the above-mentioned parameters were carefully tested and leading to a well-converged total energy. We fixed the equilibrium lattice constant for the obtained value within the traditional LDA scheme and then optimized the atomic position with an ideal U_{eff} value of 4 eV for the structure optimization. Therefore, we only considered the U_{eff} effect on the atomic interaction, ignoring its effect on the lattice parameter for the electronic-structure and thermal calculations.

3 Results and discussion

3.1 Structural properties of CeB_6

CeB_6 is one of the strongly correlated systems sharing the Pm3m structure of CaB_6 with the latest experimentally determined lattice parameter $a_0 \approx 4.132$ Å [7]. The conventional unit cell of the ClCs-type structure of CeB_6 is presented in Fig. 1. The Ce ions and B_6 octahedra are located at the corners and body center of the cubic lattice, respectively. The lattice parameter a_0 and bulk modulus B were obtained by fitting our energy-volume data to the BirchMurnaghan equation for the state [29]. Table 1 presents the lattice constant of CeB_6 according to a popular theoretical calculation and experiment. The previous theoretical results underestimate or overestimate a_0, especially compared with the latest experimental result [7]. However, our calculated lattice parameter a_0 was 4.121 Å ($U_{eff} = 0$ eV), which has discrepancies of approximately 0.27% and 0.46% compared with the experimental values of 4.132 [7] and 4.140 Å [28], respectively. Our result is in good agreement with both of the experimental results and agrees far more closely with the latest one. Figure 2 illustrates the dependence of the lattice parameter and bulk modulus on U_{eff} in the range of 0–9 eV. Clearly, the GGA calculations exhibit a somewhat longer a_0 and smaller bulk modulus B, causing a slightly less accurate description of the structural properties. Overall, the LDA yields a better agreement with the lattice parameter and bulk modulus. There is a stable increase in the lattice parameter with U_{eff} for both the LDA and GGA functionals. The lattice parameter a_0 was overestimated at the simply GGA level (U_{eff} = 0 eV); thus, considering that $U_{eff} > 0$ increases the discrepancy with respect to the experiment. However, the LDA+U method behaves contrarily: the calculation

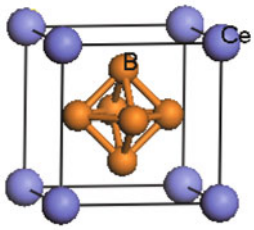

Fig. 1 The conventional unit cell of the ClCs-type structure of CeB_6. Orange and purple balls stand for B and Ce atoms, respectively.

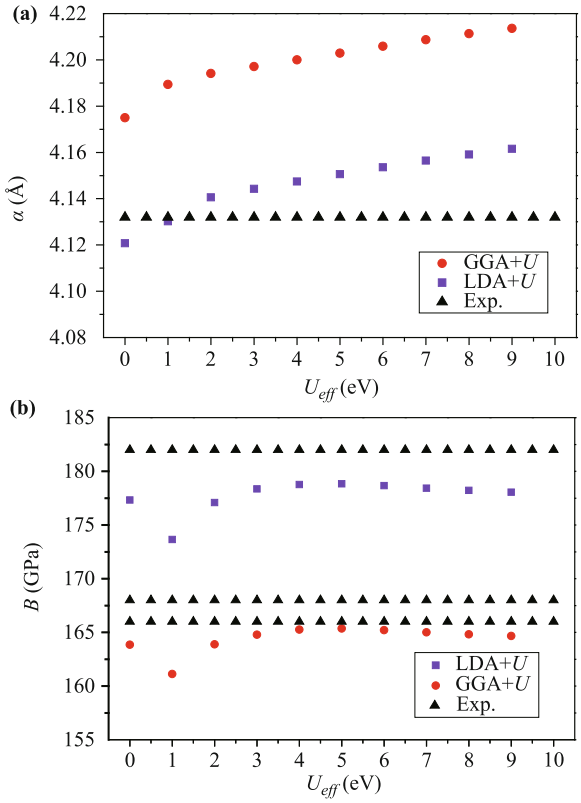

Fig. 2 Dependence of lattice parameter a_0 **(a)** and bulk modulus B **(b)** of CeB_6 on U_{eff}. Notice that for three different experimental values B can be found in the literature.

ignoring U_{eff} underestimates a_0 by ~0.011 Å compared with the experiment. Thus, it is practical to introduce U_{eff} into the calculation of the lattice constant for the LDA functional.

As shown in Fig. 2(b), the bulk modulus distinctively increased with U_{eff} from 1 to 4 eV, but decreased slightly from 4 to 9 eV, suggesting that this variable is less sensitive to higher values of U_{eff}. The bulk modulus values from the LDA calculation with the above mentioned range of U_{eff} are primarily located within 166–191 GPa [8, 9, 34], which offers better consistency with the experiment than the GGA values. For a certain U_{eff} value around 4 eV, both a_0 and B yield a well-balanced agreement with the experiment. Hence, we used the LDA+U method to study the electronic, elastic, and thermal properties of CeB_6 with an optimal U_{eff} of 4 eV.

Table 1 Calculated and experimental lattice parameter a_0 (Å), bulk modulus B (GPa), pressure derivative of the bulk modulus B' (GPa), and elastic constants C_{ij} (GPa) of CeB_6 at 0 K and 0 GPa.

Method	Ref.	a_0	B	B'	C_{11}	C_{12}	C_{44}
This work		4.121	167	3.53	483	10	75
Calc.	[11]	4.098					
Calc.	[15]	4.154	173	3.91	452	34	98
Expt.	[7]	4.132					
Expt.	[8]		168		473	16	81
Expt.	[8]		182		508	19	79
Expt.	[9]		191		472	53	78
Expt.	[10]				406	–93	78
Expt.	[28]	4.140					
Expt.	[30]		166	3.15			

3.2 Elastic properties

The bulk modulus B varied over a broad range, with values including 166 [30], 191 [9], 168, and 182 GPa [8] among the three experimental results. Our results are consistent with two experimental results [8, 30] and slightly lower than another two experimental results [8, 9]. Our calculated pressure derivative of the bulk modulus B' agrees better with the experimental result [30] than that with the recent theoretical result [15]. The elastic constant C_{11} is in agreement with the results of Refs. [8] and [9], and C_{44} is consistent with the results of Refs. [8], [9], and [10]. For the controversial elastic constant C_{12}, our results validate the experimental results of Lüthi *et al.*, exhibiting no negative values. We predict that the most probable value of C_{12} tends to be >10 GPa. Overall, our calculated elastic constants agree better with the experimental results than that with the recent theoretical results obtained using the ABINIT code [31].

It seems insignificant that elastic and thermal properties are studied with respect to the effects of U_{eff}, as this method is mainly proposed for studying the electronic structure of strongly correlated systems. Thus, we examined both properties under pressure with an optimal U_{eff} value of 4 eV. The elastic properties of a material help determine its Debye temperature and mechanical stability. The calculated and experimental bulk modulus B (GPa) and elastic constants C_{ij} (GPa) at 0 K and 0 GPa are listed in Table 1. To the best of our knowledge, the computation of the bulk modulus using the stress tensor yields a slightly less precise bulk modulus because of the Pulay stress because of the incompleteness of the plane-wave basis set. However, our results for

0 K and 0 GPa agree with the experimental results and other theoretical data because of the sufficiently accurate approximation.

Table 2 Calculated bulk modulus B (GPa), shear modulus G (GPa), Young's modulus E (GPa), Poisson's ratio σ, B/G values, longitudinal acoustic velocities V_L (km/s), shear acoustic velocities V_S (km/s), and Debye temperature Θ_E (K) of CeB_6 under pressure.

P	B	G	B/G	E	σ	V_S	V_L	Θ_E
0	166.8	121.2	1.38	482.7	0.018	4.95	8.15	760
10	201.8	132.7	1.52	548.5	0.047	5.05	8.54	790
20	234.7	139.2	1.69	607.0	0.069	5.07	8.81	806
30	267.2	150.3	1.78	660.2	0.088	5.17	9.12	834
40	298.8	158.3	1.89	712.8	0.103	5.22	9.37	852
50	326.5	175.3	1.86	756.7	0.114	5.41	9.67	892
60	362.3	176.1	2.06	806.6	0.129	5.35	9.85	892
70	390.8	186.3	2.10	849.4	0.138	5.43	10.06	914
80	428.8	193.1	2.22	896.5	0.152	5.47	10.31	928
90	451.4	198.8	2.27	934.2	0.155	5.49	10.42	939
100	479.0	209.6	2.29	973.1	0.161	5.58	10.61	960
110	508.5	219.1	2.32	1012.4	0.168	5.64	10.79	979
120	542.7	227.1	2.39	1051.8	0.177	5.69	10.99	994

Figure 3 shows the pressure dependence of the elastic constants from 0 to 120 GPa. Here, C_{11} varies largely according to the applied pressure compared with C_{12} and C_{44}, indicating that C_{12} and C_{44} are less sensitive to the pressure than C_{11}. In the wide pressure range of 0–120 GPa, the elastic constants C_{11}, C_{12}, and C_{44}, the bulk modulus B, and the shear modulus Gincreased monotonically with pressure, but C_{44} was relatively stable and had a similar variation trend to the shear modulus G. A similar variation phenomenon is also observed for C_{11} and C_{12} in the comparable structure CaB_6 [32], but C_{44} has some differences. The C_{44} of CeB_6 varies from 75 to 139 GPa, whereas that of CaB_6 is relatively stable, remaining within 43–46 GPa.

Table 2 presents our calculated bulk modulus B, shear modulus G, Young's modulus E, Poisson's ratio σ, B/G values, longitudinal acoustic velocities V_L, shear acoustic velocities V_S, and Debye temperature Θ_E of CeB_6 under hydrostatic pressure in the range of 0–120 GPa at 0 K. The bulk modulus and shear modulus indirectly indicate the hardness [33]. Generally, a superhard material has a high bulk modulus, high shear modulus, and high shear strength. Thus, we predict that CeB_6 has high hardness. Table 2 shows that the bulk modulus B increased gradually with the increasing pressure, demonstrating that the CsCl-type structure CeB_6 became more difficult to compress as the pressure increased. A high (low) B/G value is associated with ductility (brittleness), and the critical value that separates ductile and brittle materials is ~1.75. Overall, the calculated B/G values increased with pressure, and the pressure at which this substance transformed from brittle to ductile was predicted as 27 GPa. The pressure can undoubtedly improve the ductility of a material. The Young's modulus E is used to determine the stiffness of solids. A stiff material has a large E. Information about the bonding force can be obtained using Poisson's ratio σ. The Young's modulus E and Poisson's ratio σ are defined as

$$E = \frac{9BG}{3B+G}, \quad \sigma = \frac{1}{2}\left(\frac{3B-2G}{3B+G}\right). \tag{2}$$

At the ground state, E = 482.7 GPa. As the applied pressure increases, E gradually increases, demonstrating that the pressure enhances the stiffness of the substance. The Poisson's ratio σ is 0.018 at 0 GPa, indicating that the inter-atomic forces within CeB_6 are non-central, as the low limit of Poisson's ratio σ for central-force solids is 0.25 [34]. As the pressure increases, the remaining Poisson's ratio σ remains less than 0.25, suggesting that the inter-atomic forces in CeB_6 are non-central at higher pressures. Additionally, many crystals present elastic anisotropies to some extent. The percentages of the compression anisotropy A_{comp} and shear anisotropy A_{shear} are defined as [35]

$$A_{comp} = \frac{B_V - B_R}{B_V + B_R} \times 100\%,$$
$$A_{shear} = \frac{G_V - G_R}{G_V + G_R} \times 100\%. \tag{3}$$

The maximum and minimum values of A_{comp} and A_{shear} are 100% and 0%, respectively. A zero value indicates isotropy, whereas 100% indicates maximum anisotropy. At the ground state of CeB_6, A_{comp} is 0, and A_{shear} is 15.21%, indicating that there is isotropy in compression, but anisotropy in shear. The mechanical-stability conditions in cubic structures can be expressed with regard to the elastic constants as

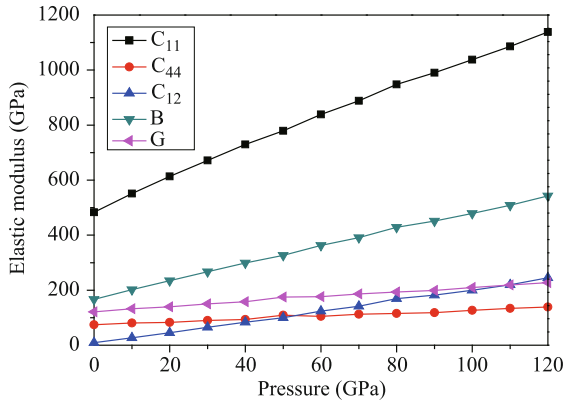

Fig. 3 Pressure dependence of elastic constants of CsCl-type structure from 0 GPa to 120 GPa at 0 K from LDA+U calculations with U = 4 eV.

$$\tilde{C}_{44} > 0, \quad \tilde{C}_{11} > \left|\tilde{C}_{12}\right|, \quad \tilde{C}_{11} + 2\tilde{C}_{12} > 0, \tag{4}$$

where $\tilde{C}_{ii} = C_{ii} - P(i = 1, 4)$, and $\tilde{C}_{12} = C_{12} + P$. A strong increase in the temperature dependence of the resistance at 122 GPa was reported, which may signify a structural change around 85–122 GPa [7]. All the elastic constants given in Fig. 3 satisfy these stability conditions, indicating that CeB_6 remains mechanically stable up to 120 GPa.

3.3 Sound velocities and thermal properties

The Debye temperature is an important fundamental quantity that is closely related to many physical properties of solids, such as the specific heat and melting temperature. Above the Debye temperature, the quantum effects can be ignored, whereas below the Debye temperature, the quantum mechanical effects are very important for understanding the thermal properties of materials. According to the quasi-harmonic Debye model [36], we can obtain the Debye temperature Θ_D of CeB_6 under different pressures and temperatures. In the quasi-harmonic Debye model, the non-equilibrium Gibbs energy under a pressure p and temperature T is written as

$$G^*(V; p; T) = E(V) + pV + A_{vib}(\Theta_D(V); T), \tag{5}$$

where $E(V)$ is the total energy per formula unit, pV corresponds to the constant hydrostatic-pressure condition, A_{vib} is the vibrational Helmholtz free energy, and Θ_D is the Debye temperature Θ_D, which is given as

$$\Theta_D = \frac{\hbar}{k}(6\pi^2 V^{1/2} n)^{1/3} f(\sigma)\sqrt{\frac{B_s}{M}}, \tag{6}$$

with the assumption of an isotropic solid having Poisson's ratio σ. Here, M is the molecular mass per formula unit, B_s is the adiabatic bulk modulus, and $f(\sigma)$ is given as

$$f(\sigma) = \left\{3\left[2\left(\frac{2}{3}\frac{1+\sigma}{1-2\sigma}\right)^{3/2} + \left(\frac{1}{3}\frac{1+\sigma}{1-\sigma}\right)^{3/2}\right]^{-1}\right\}^{1/3}. \tag{7}$$

Additionally, the elastic Debye temperature [37] can be obtained using the elastic constants. The Debye temperature Θ_E is estimated as

$$\Theta_E = \frac{h}{k}\left[\frac{3n}{4\pi}\left(\frac{N_A\rho}{M}\right)\right]^{1/3} V_m, \tag{8}$$

where h is Planck's constant, k is Boltzmann's constant, N_A is Avogadro's number, n is the number of atoms per formula unit, $M$is the molecular mass per formula unit, ρ is the density, and V_m is obtained as [38]

$$V_m = \left[\frac{1}{3}\left(\frac{2}{V_S^3} + \frac{1}{V_L^3}\right)\right]^{-1/3}. \tag{9}$$

Here, V_S and V_L are the shear and longitudinal sound velocities, respectively. The probable values of the average shear and longitudinal sound velocities can be calculated using Navier's equations as follows [39]:

$$V_S = \sqrt{\frac{G}{\rho}} \quad , V_L = \sqrt{\frac{B + (4/3)G}{\rho}}. \tag{10}$$

Here, a Cauchy solid ratio of 0.25 is used as Poisson's ratio σ.

The obtained shear and longitudinal sound velocities are 4.95 and 8.15 km/s, respectively, at 0 K and 0 GPa (Table 2). Clearly, the shear sound velocities increase slowly, and the longitudinal sound velocities increase relatively quickly. These effects are associated with the shear anisotropy and compression isotropy, respectively. Because the sound velocities are directly proportional to the elastic modulus of the medium, the shear and longitudinal sound velocities exhibit variation trends quite similar to those of the shear modulus G and elastic modulus E, respectively.

To obtain typical and persuasive energy-volume data points for the thermal-property calculation, every energy value at the corresponding volume was obtained from the novel point of the U_{eff} effect on the atomic interaction. According to the quasi-harmonic Debye model, the bulk modulus B is 181.3 GPa, which agrees with the experimental value of 182 GPa [8], confirming the validity of our results. Here, the Debye temperature Θ_D was 718 K at 0 K and 0 GPa, which agrees with the previously obtained elastic Debye temperature Θ_E = 760 K for CeB_6. The Debye temperature increased monotonically with pressure up to 100 GPa (Fig. 4). With pressure below 12 GPa, the difference between the two Debye

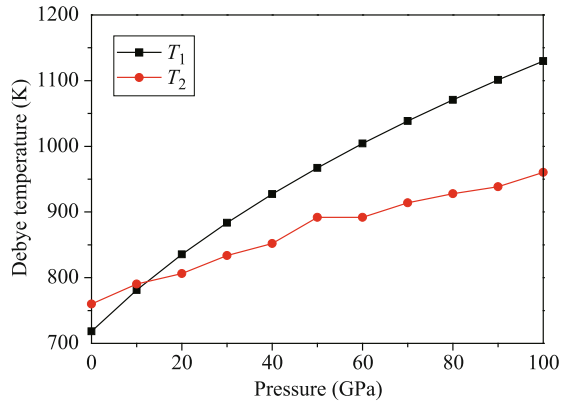

Fig. 4 Pressure dependence of the Debye temperature Θ_D (T_1) calculated by thermodynamic methods and elastic Debye temperature Θ_E(T_2) of CsCl-type structure CeB_6 at 0 K from LDA+U calculations with U = 4 eV.

temperatures decreased. However, at higher pressures—especially above 50 GPa—this difference increased. This suggests that the anisotropy of the cubic structure decreased before 12 GPa and increased after 12 GPa, which is consistent with the fluctuation of the shear anisotropy A_{shear} under pressure. This is partially because the Debye temperature Θ_D was obtained under the assumption that the material was isotropic.

3.4 Electronic structures and magnetic properties

We focused on studying the electronic structure by analyzing the DOS with different values of U_{eff} and pressure. The DOS plays an important role in the analysis of the physical properties of materials. To precisely determine the energy positions of Ce-4f with respect to the Fermi level, we illustrate the calculated DOS with different approximations (LDA, LDA+U with $U = 4$ eV, and LDA+U with $U = 8$ eV) in Fig. 7(a). Obviously, the main peak of the Ce-4$f$states was located at 0.5 eV in the conduction band, which is not in good agreement with the experimental result. According to Neupane *et al.*, the peak is located around 2 eV in the conduction band [16]. The inappropriate treatment of the Ce-4f states within the LDA scheme largely causes this error. The main peak of Ce-4f transformed toward a higher level as U_{eff} increased. When the position of the Ce-4f peak was consistent with that of the experiment, as shown in Fig. 7(a), the obtained value of U_{eff} also agrees well with that reported in Ref. [13]. Thus, it is reasonable to calculate the physical properties with an optimal U_{eff} value of 4 eV.

Sandeep *et al.* [13] calculated the magnetic moment of CeB_6 as 1.03 u_B, which agrees with the results of Singh *et al.* [40]. Our results for the magnetic moment of the system, originating from the spin of the Ce atom, also indicate a value of 1.03 u_B at 0 GPa, whereas the magnetic moment decreased slightly to 0.97 u_B at 85 GPa. In magnetic materials, anti-parallel coupling between the magnetic moment and conduction electrons yields a non-magnetic Fermi liquid phase, which is known as the Kondo effect. Using neutron-diffraction experiments on CeB_6 single crystals, Rossat-Mignod *et al.* [41] detected that there is a homogeneous moment reduction because of the Kondo effect in low-temperature phase III. This reduction is consistent with our results. A comparison between Figs. 5(a) and (b) suggests that through the general shapes of the DOS for both spin directions, the magnetic moment did not vary significantly with pressure. There was a decrease in the intensity of the peaks with an absence of the DOS in the energy range of 7.5–17.5 eV at 85 GPa compared with that at 0 GPa. There was also a new small peak for spin-up electrons, which may cause the formation of the magnetic moment at this pressure.

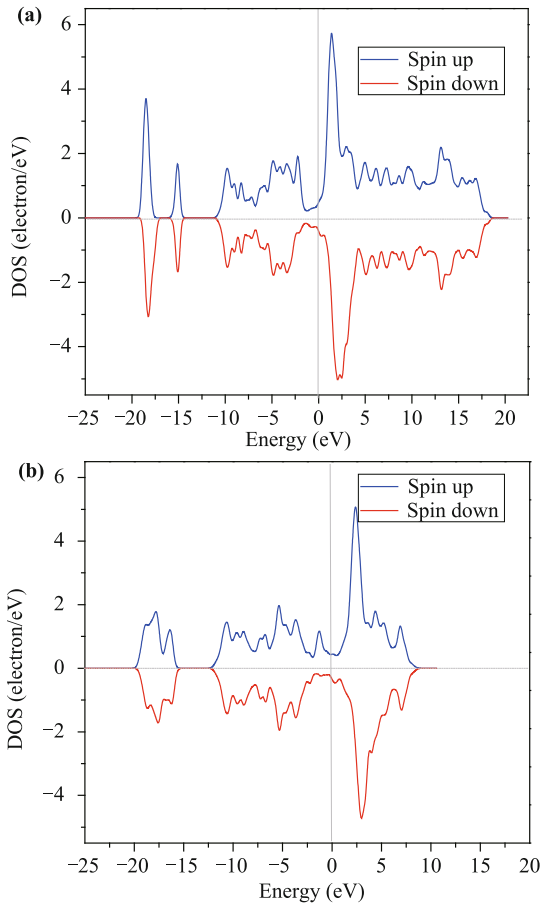

Fig. 5 The projected DOS for spin-up and spin-down electrons of CeB_6 at 0 GPa **(a)** and 85 GPa **(b)** from LDA+U calculations with $U = 4$ eV.

Figure 6 depicts the band structures of spin-down and spin-up electrons at 0 GPa. Obviously, there is no bandgap between the conduction band minimum (CBM) and valence band maximum (VBM) for spin-up electrons, whereas there is a small gap for spin-down electrons. According to recent experiments by Neupane *et al.* [16], the Fermi surface of CeB_6 comprises large oval-shape pockets at the X points within the Brillouin zone, and the Ce quasi-particle states participate in the formation of hotspots at the Fermi surface, yielding an overlap between the CBM and VBM around the X points. The antibonding states, comprising the most localized Ce-4f states, have the smallest interaction with the neighboring atoms and thus have the smallest energy spread. Consequently, the un-localized Ce-5$d$states and localized Ce-4f states correspond to the dispersive bands and flat bands, respectively. In Fig. 6, we observe dispersive Ce-5d bands and flat Ce-4f bands in the vicinity of the Fermi level with the Ce-5d and 4f states across the Fermi level

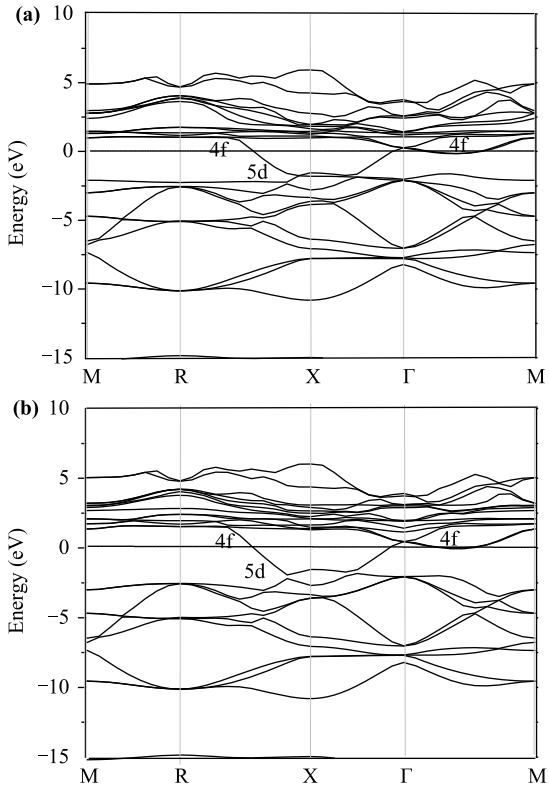

Fig. 6 The bulk band structure along the high-symmetry direction M-R-X-Γ-M at 0 GPa from LDA+U calculations with $U = 4$ eV; **(a)** is for spin-up electrons and **(b)** is for spin-down electrons.

along the high-symmetry direction. Moreover, one additional energy band appears in the valence band shown in Fig. 6(a) compared with that shown in Fig. 6(b), which agrees with the case where spin-up electrons contribute more to the DOS than spin-down electrons, as shown in Fig. 5(a). Our results show that the Ce-4f band is mainly above the Fermi level in the conduction band, whereas the ARPES data show that the 4f states are below the Fermi level. There are two reasons for this discrepancy: i) ARPES only measures the states below the Fermi level; ii) the theoretical band structure indicates that the maximum weight of the f bands are above the Fermi level [16], which agrees with our calculated DOS and band structure. One cannot exclude the possibility that the 4f states are above the Fermi level.

Figure 7 shows the calculated total DOS (TDOS) and partial DOS (PDOS) at 0 and 85 GPa. At both pressures, the DOS in the vicinity of the Fermi level is predominated by the Ce-4f and Ce-5d states. The typical characteristic of the TDOS for transition-metal borides may be what is regarded as a pseudogap (a sharp valley around the Fermi level) [42], which appear in crystalline solids [43], amorphous alloys [44], and quasi-crystals [45]. The two mechanisms were proposed for the formation of pseudogap in binary alloys. One is of ionic origin, and the other involves a hybridization effect. However, there is no noticeable pseudogap in CeB_6 and no distinctive hybridized peak between the Ce 4f+5d states and B 2p states shown in Fig. 7, which indicates the weakness of the covalent bonding between these two types of atoms. According to the atomic Mulliken population shown in Table 3, 2.34 and 2.72 electrons are transferred from Ce to B at 0 and 85 GPa, respectively, indicating that the Ce-B bonds have more distinctive ionic characteristics at 85 GPa. The electronegativity difference between Ce and B is high; hence, the ionicity strongly affects the bonding behavior. To further clarify the bonding property, the total charge densities at different pressures are shown in

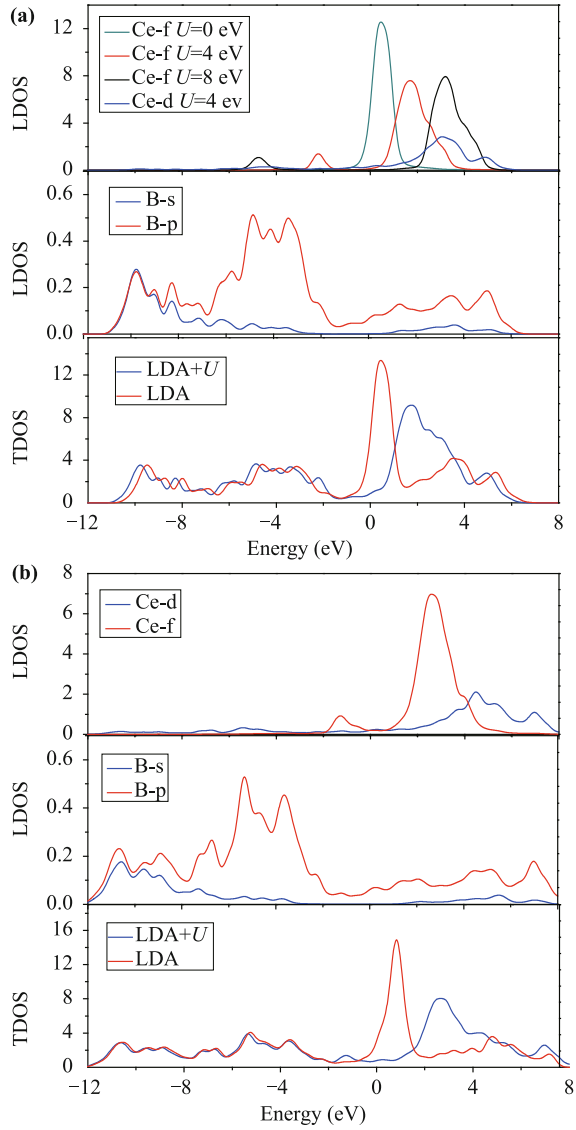

Fig. 7 The CsCl-type structure CeB_6 calculated total and local DOS, TDOS and LDOS from LDA+U calculations with $U = 4$ eV, at 0 GPa **(a)** and 85 GPa **(b)**, respectively; The Ce-f component of the TDOS at 0 GPa is calculated with three different approximations: LDA, LDA+U with $U = 4$ eV and LDA+U with $U = 8$ eV.

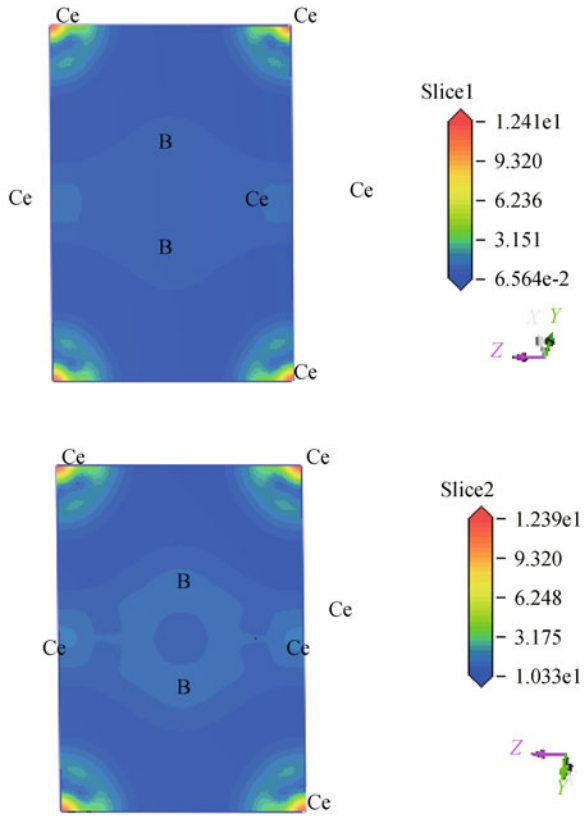

Fig. 8 The charge density difference of CeB_6 for a selected (110) plane from LDA+U calculations with $U = 4$ eV; Slice 1 is at 0 GPa and Slice 2 is at 85 GPa.

Fig. 8. Clearly, the electrons gradually accumulated at the B atoms and Ce atoms at 85 GPa compared with 0 GPa, suggesting that the charge transfer still dominates the bonding at a high pressure. This result agrees well with the population analysis.

It is clear that the traditional LDA method incorrectly predicts the DOS of CeB_6 in the vicinity of the Fermi level, making the peak of DOS closer to the Fermi level. According to Fig. 7, the inclusion of the Hubbard U term in the LDA functional causes the peak of the DOS to shift away from the Fermi level and moves the energy ranges of Ce $5d$+$4f$ states to the higher-energy region in the conduction band. This also occurs at 85 GPa. We can observe the difference in the DOSs of CeB_6 between 0 and 85 GPa. First, at 85 GPa, the TDOS and PDOS decrease over the entire range of their distribution. Second, the valence band and conduction band broaden at 85 GPa. Moreover, the peak at the bottom of the conduction band moves to the higher-energy region compared with that at 0 GPa. In conclusion, we find it interesting that the mechanism of high pressure is similar to that of increasing U_{eff} because the peaks at the bottom of conduction band move to the high-energy region in both cases.

Table 3 Mulliken atomic orbital population (s, p, d, f), total population (Total), charge transferred (Charge) (unit: e) and spin magnetic moment (Moment) (unit: u_B) of CeB_6 under pressure P (GPa).

P	Species	s	p	d	f	Total	Charge	Moment
0	B	0.82	2.57	0.00	0.00	3.39	–0.39	0.00
0	Ce	1.82	5.22	1.48	1.14	9.66	2.34	1.06
85	B	0.72	2.73	0.00	0.00	3.45	–0.45	0.00
85	Ce	1.63	4.80	1.68	1.17	9.28	2.72	1.00

4 Conclusions

We evaluated the structural, elastic, and electronic properties of the Kondo compound CeB_6 by using the LDA+U method according to density functional theory. It seems reasonable to conduct calculations of the physical structure and properties with an optimal U_{eff} value of 4 eV. Our calculated lattice constant and elastic constants are in good agreement with the experimental results and other theoretical findings. The U_{eff} dependence of the lattice constant and bulk modulus, as well as the elastic constants under pressure, were investigated for the first time. The important conclusions of our calculations are as follows. i) There was a stable increase in the lattice parameter as U_{eff} increased, whereas the bulk modulus was less sensitive to higher values of U_{eff} for both the LDA and GGA functionals. ii) The pressure at which this substance transformed from brittle to ductile was predicted as 27 GPa. In contrast to experiments speculating the possibility of a structural change in the range of 85–122 GPa, our results indicate that CeB_6 is mechanically stable up to 120 GPa. iii) We estimated a Debye temperature Θ_D of 718 K using thermodynamic methods, which is close to the elastic Debye temperature Θ_E of 760 K obtained with elastic constants at 0 K and 0 GPa. iv) The magnetic moment of this system was insensitive to the pressure, according to the calculations and TDOS analysis. The Ce-B bonds had a more distinctive ionic characteristic at 85 GPa than at 0 GPa. The mechanism of high pressure is similar to that of the increase in U_{eff} for the movement of the peak to the high-energy region at the bottom of the conduction band.

Acknowledgements The authors would like to thank the support by the National Natural Science Foundation of China (Grant No. 11204192). We also acknowledge the support for the computational resources by the State Key Laboratory of Polymer Materials Engineering of China in Sichuan University.

References and notes

1. C. Loschen, J. Carrasco, K. M. Neyman, and F. Illas, First-

principles LDA+ U and GGA+ U study of cerium oxides: Dependence on the effective U parameter, *Phys. Rev. B* 75(3), 035115 (2007)

2. Y. Y. Qi, Z. W. Niu, C. Cheng, and Y. Cheng, Structural and elastic properties of Ce_2O_3 under pressure from LDA+U method, *Front. Phys.* 8(4), 405 (2013)
3. W. Li, C. Setty, X. H. Chen, and J. P. Hu, Electronic and magnetic structures of chain structured iron selenide compounds, *Front. Phys.* 9(4), 471 (2014)
4. O. Zaharko and P. Fischer, Zero-field magnetic structure in CeB_6 reinvestigated by neutron diffraction and muon spin relaxation, *Phys. Rev. B* 68(21), 214401 (2003)
5. D. Hall and Z. Fisk, Magnetic-field dependence of the high-temperature magnetically ordered phase transition in CeB_6, *Phys. Rev. B* 62(1), 84 (2000)
6. R. G. Goodrich, D. P. Young, D. Hall, L. Balicas, Z. Fisk, and N. Harrison, Extension of temperature-magnetic field phase diagram of CeB_6, *Phys. Rev. B* 69(5), 054415 (2004)
7. N. Foroozani, J. Lim, G. Fabbris, P. F. S. Rosa, Z. Fisk, and J. S. Schilling, Suppression of dense Kondo state in CeB_6 under pressure, *Physica B* 457, 12 (2015)
8. B. Lüthi, S. Blumenroder, B. Hillebrands, E. Zirngiebl, G. Güntherodt, and K. Winzer, Elastic and magnetoelastic effects in CeB_6, *Z. Phys. B: Condens. Matter* 58(1), 31 (1984)
9. S. Nakamura, T. Goto, S. Kunii, K. Iwashita, and A. Tamaki, Quadrupole-strain interaction in rare earth hexaborides, *J. Phys. Soc. Jpn.* 63(2), 623 (1994)
10. T. Goto, A. Tamaki, S. Kunii, T. Nakajima, T. Fujimura, T. Kasuya, T. Komatsubarra, and S. B. Woods, Elastic properties in CeB_6, *J. Magn. Magn. Mater.* 31, 419 (1983)
11. C.J. Pickard, B. Winkler, R. K. Chen, M.C. Payne, and D. Vanderbilt, Structural properties of Lanthanide and Actinide compounds within the Plane Wave Pseudopotential Approach, *Phys. Rev. Lett.* 85(24), 5122 (2000)
12. W. Sikora, F. Bialas, L. Pytlik, and J. Malinowski, Symmetry analysis of antiferroquadrupolar order and accompanying atomic displacements in CeB_6, *Solid State Sci.* 7(6), 645 (2005)
13. Sandeep, M. P. Ghimire, D. P. Rai, P. K. Patra, and R. K. Thapa, Study of Bulk modulus, Volume, Energy, latticeparameters and magnetic moments in rare earth hexaborides using density functional theory, *J. Phys.: Conf. Ser.* 377(1), 012084 (2012)
14. T. G. Liu, W. Q. Zhang, and Y. L. Li, First-principles study on the structure, electronic and magnetic properties of $HoSi_n$ (n= 1–12, 20) clusters, *Front. Phys.* 9(2), 218 (2014)
15. T. Gürel and R. Eryiğit, An initio lattice dynamics and thermodynamics of rare-earth hexaborides LaB_6 and CeB_6, *Phys. Rev. B* 82(10), 104302 (2010)
16. M. Neupane, N. Alidoust, G. Bian, S.Y. Xu, and P. P. Shibayev et al., Fermi surface topology and hotspots distribution in Kondo lattice system CeB_6, arXiv: 1411.0302 (2014)
17. S. Fabris, S. de Gironcoli, S. Baroni, G. Vicario, and G. Balducci, Taming multiple valency with density functionals: A case study of defective ceria, *Phys. Rev. B* 71(4), 041102 (2005)
18. G. Kresse, P. Blaha, J. L. F. Da Silva, and M. V. Ganduglia Pirovano, Comment on "Taming multiple valency with density functionals: A case study of defective ceria", *Phys. Rev. B* 72(23), 237101 (2005)
19. S. V. Demishev, A. V. Semeno, A. V. Bogach, N. A. Samarin, T. V. Ishchenko, V. B. Filipov, N. Y. Shitsevalova, and N. E. Sluchanko, Magnetic spin resonance in CeB_6, *Phys. Rev. B* 80(24), 245106 (2009)
20. P. Schlottmann, Electron spin resonance in antiferroquadrupolar-ordered CeB_6, *Phys. Rev. B* 86(7), 075135 (2012)
21. M. C. Payne, M. P. Teter, D. C. Allan, T. A. Arias, and J. D. Joannopoulos, Iterative minimization techniques for ab initio total-energy calculations: Molecular dynamics and conjugate gradients, *Rev. Mod. Phys.* 64(4), 1045 (1992)
22. V. Milman, B. Winkler, J. A. White, C. J. Packard, M. C. Payne, E. V. Akhmatskaya, and R. H. Nobes, Electronic structure, properties, and phase stability of inorganic crystals: A peeudopotential plane-wave study, *Int. J. Quant. Chem.* 77(5), 895 (2000)
23. S. H. Vosko, L. Wilk, and M. Nusair, Accurate spin-dependent electron liquid correlation energies for local spin density calculations: A critical analysis, *Can. J. Phys.* 58(8), 1200 (1980)
24. V. I. Anisimov, I. V. Solovyev, and M. A. Korotin, Density-functional theory and NiO photoemission spectra, *Phys. Rev. B* 48(23), 16929 (1993)
25. M. Cococcioni and S. de Gironcoli, Linear response approach to the calculation of the effective interaction parameters in the LDA+U method, *Phys. Rev. B* 71(3), 035105 (2005)
26. H. J. Monkhorst and J. D. Pack, Special points for Brillouin-zone integrations, *Phys. Rev. B* 13(12), 5188 (1976)
27. G. Kresse and J. Furthmüller, Efficiency of ab-initio total energy calculations for metals and semiconductors using a plane-wave basis set, *Comput. Mater. Sci.* 6(1), 15 (1996)
28. S. Sato, A spherical charge distribution in a crystal of CeB_6, *J. Magn. Magn. Mater.* 52(1–4), 310 (1985)
29. F. Birch, Finite elastic strain of cubic crystals, *Phys. Rev.* 71(11), 809 (1947)
30. J. M. Leger, J. Rossat-Mignod, S. Kunii, and T. Kasuya, High pressure compression of CeB_6 up to 20 GPa, *Solid State Commun.* 54(11), 995 (1985)
31. X. Gonze, et al., ABINIT: First-principles approach to material and nanosystem properties, *Comput. Phys. Commun.* 180(12), 2582 (2009)
32. Y. K. Wei, J. X. Yu, Z. G. Li, Y. Cheng, and G. F. Ji, Elastic and thermodynamic properties of CaB_6 under pressure from first principles, *Physica B* 406(23), 4476 (2011)
33. D. M. Teter, Computational alchemy: The search for new superhard materials, *Mrs. Bulletin* 23(01), 22 (1998)

34. F. Chu, Y. He, D. J. Thoma, and T. E. Mitchell, Elastic constants of the C_{15} laves phase compound $NbCr_2$, *Scr. Metal. Mater.* 33(8), 1295 (1995)
35. K. B. Panda and K. S. Ravi Chandran, Determination of elastic constants of titanium diboride (TiB_2) from first principles using FLAPW implementation of the density functional theory, *Comp. Mater. Sci.* 35(2), 134 (2006)
36. M. A. Blanco, E. Francisco, and V. Luaña, *Comput. Phys. Commun.* 158(1), 57 (2004)
37. W. A. Harrison, Elastic Structure and Properties of Solids, Freeman and Company, San-Francisco, 1980
38. O. L. Anderson, A simplified method for calculating the debye temperature from elastic constants, *J. Phys. Chem. Solids* 24(7), 909 (1963)
39. R. Hill, The elastic behavior of a crystalline aggregate, *Proc. Soc. London. A* 65(5), 349 (1952)
40. N. Singh, S. M. Saini, T. Nautiyal, and S. Auluck, Electronic structure and optical properties of rare earth hexabordes RB_6 (R = La, Ce, Pr, Nd, Sm, Eu, Gd), *J. Phys.: Condens. Matter* 19(34), 346226 (2007)
41. J. Rossat-Mignod, P. Burlet, T. Kasuya, S. Kunii, and T. Komatsubara, Evidence for a modulated ordering in CeB_6 due to the Kondo effect, *Solid State Commun.* 39(3), 471 (1981)
42. P. Vajeeston, P. Ravindran, C. Ravi, and R. Asokamani, Electronic structure, bonding, and ground-state properties of AlB_2-type transition-metal diborides, *Phys. Rev. B* 63(4), 045115 (2001)
43. J. H. Xu, and A. J. Freeman, Phase stability and electronic structure of $ScAl_3$ and $ZrAl_3$ and of Sc-stabilized cubic $ZrAl_3$ precipitates, *Phys. Rev. B* 41(18), 12553 (1990)
44. A. Pasturel, C. Colinet, and P. Hicter, Strong chemical interactions in disordered alloys, *Physica B & C* 132(2), 177 (1985)
45. J. C. Phillips, Structure and electronic pseudogaps of stable quasicrystals, *Phys. Rev. B* 47(5), 2522 (1992)